INFONET Seminar Application Group

Two-dimensional ultrasound detection with unfocused frequency-randomized signals

Gregory T. Clement

Presenter Pavel Ni

Outline

- Background
- Introduction
- Theory
- Simulation model
- Results
- Conclusion

Background

General US imaging use bandwidth and frequency to determine image resolution

- High frequency –> narrower beam –> better resolution
- High frequency –> higher beam attenuation –> lack of deep imaging

Therefor present US technique turned to increasingly grows of frequency range. Current frequencies for medical imaging is 2-20 MHZ

Introduction

Technique should be turned from focused to unfocused to escape frequency grows

- For each element randomly selected individual frequencies, resulting signal is includes large bandwidth.
- Single point is used to record time history
- Reconstruction of ROI is performed from analysis of acquired signal from single element
- Process is repeated with different frequency patterns to increase performance of reconstruction
- Signal analysis consists of a Fourier-based approach

Theory

- First emitter approximated as an array of simple sources radiating on unique frequency.
- Another approximation that we can describe pressure at any point in a homogeneous space given by

$$p_w(r,t) = -ic_0 k_0 \rho_0 S_w g_w(r_{s_w} | r_0), \quad (1)$$

- Acoustic pressure for wave encounters a varying density may be described

$$\rho \nabla \left(\frac{1}{\rho} \nabla p_w\right) + \frac{w^2}{c^2} p_w = 0$$

- To improve SNR process with new random frequency distribution can be repeated M-times. With M signal strength will increase linearly while noise N will further randomized

$$\tilde{\tilde{p}}_M(r', w) = Mq(r') + \sum_{m=1}^{M} N_m(r', w)$$

Theory

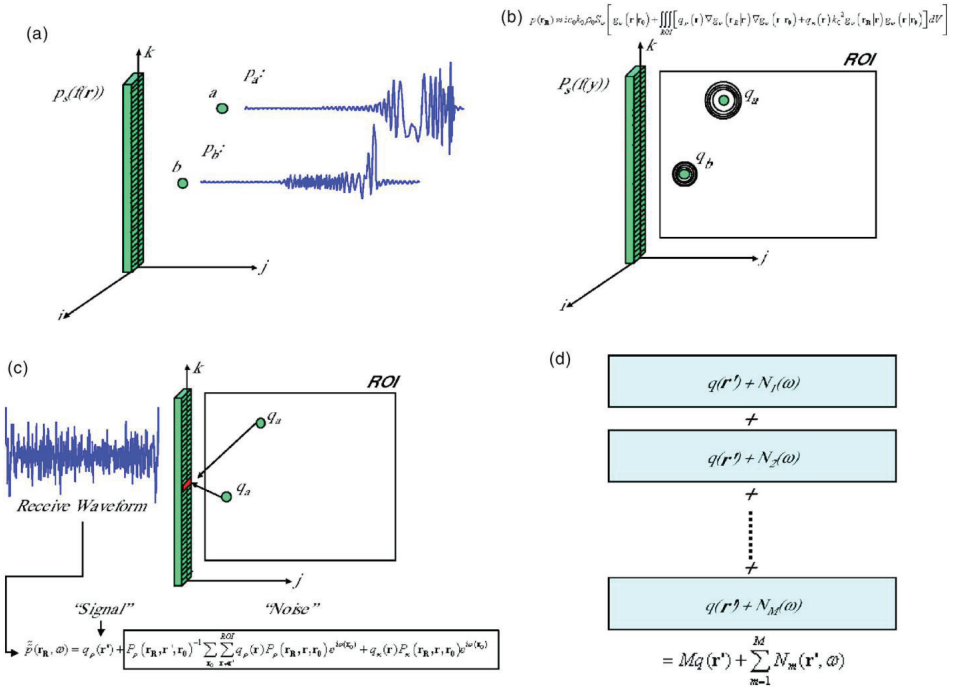

$$p(r_R, w) = q_p(r') + Pp(r_R, r', r_0)^{-1} \sum_{x_0} \sum_{x \to x^{-1}}^{ROI} q_p(r) P_\rho(r_R, r, r_0) e^{iw(x_0)} + q_k(r) P_x(r_R, r, r_0) e^{iw(x_0)}$$

'Signal' 'Noise'

Simulation model

- An operating frequency range between 0.1 – 1.25 MHz
- Simulated array is 40 mm in length and 10 mm in width
- Array segmented in to 202 linear sources with no kerf
- A linear distribution of 202 frequencies between 0.1-1.25 MHz with a frequency resolution of 5.7 kHz
- Each time randomly only one frequency assigned to element
- Also randomly single element selected to record signal
- Scattering field is placed within ROI
- Scattering signal at the receiver is discrete approximation of Eq. (10)

Results

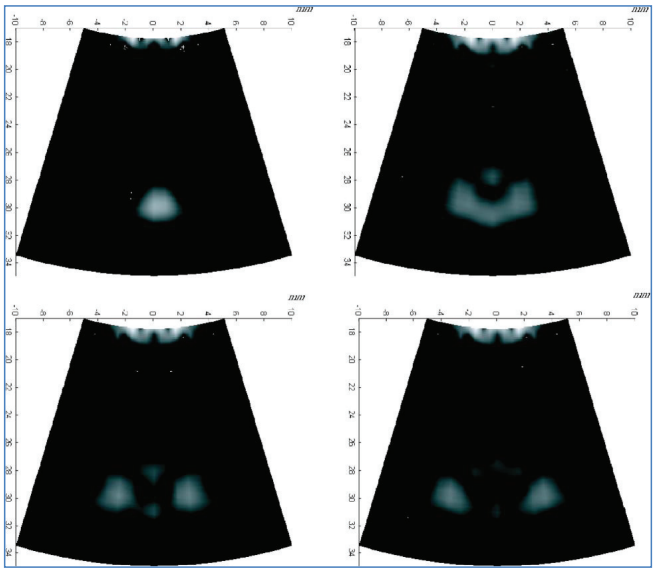

Simulated B-scan images f_c=0.67MHz. Two wires with (diam=0.2mm) separated by a) 2mm, b) 4mm, c) 6mm, d) 8mm.

- Simulated B-scan via k-space projection algorithm using 200 ns resolution. Simulation was repeated for each of 21 scan directions
- ROI 40x40 mm
- Two objects with diameter 0.2mm was given sound speed of 3500 m/s
- Only on 8mm separation objects are clearly separated

Results

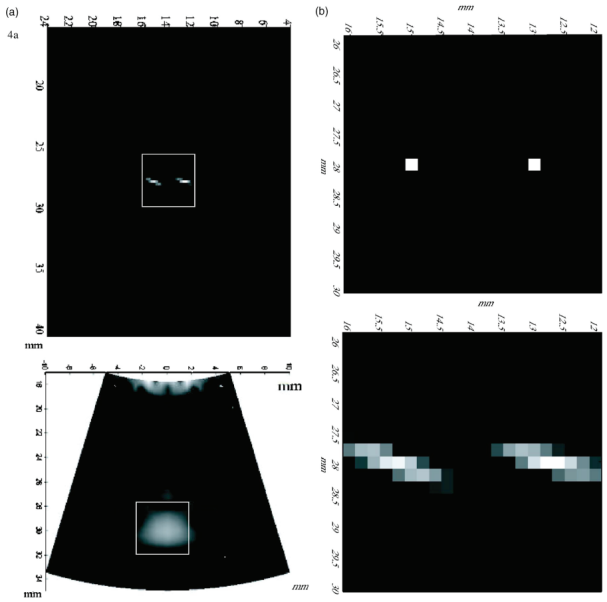

Comparison a) random frequencies (top) B-scan (bottom) b) more magnified view

- Comparing with B-scan method with randomized frequencies has better performance.
- Two objects can be imaged separately with 1.35 mm distance. Vertical 0.5mm
- Simulation was repeated with 15 randomized signals

Results

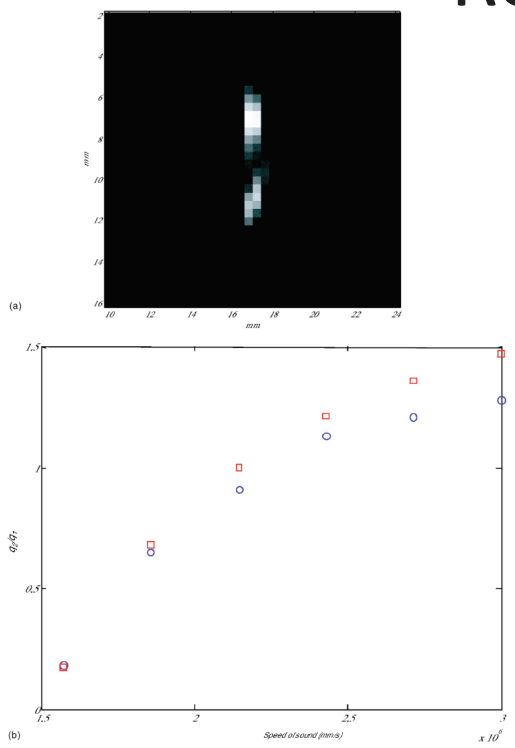

Two reconstructed objects in the ROI with scattering strengths q1= 0.51 and q2=0.62 (top) Scattering ratio of q2/q1 is plotted as fn of frequencies (squares). Reconstructed values (cycles)

- Object placed 4 mm apart and 17 mm distance from transducer
- The plot shows trend of increased distortion with higher sound speed. Corresponding error ranged from 4.3% at 1857 m/s to 13% at 3000 m/s

Results

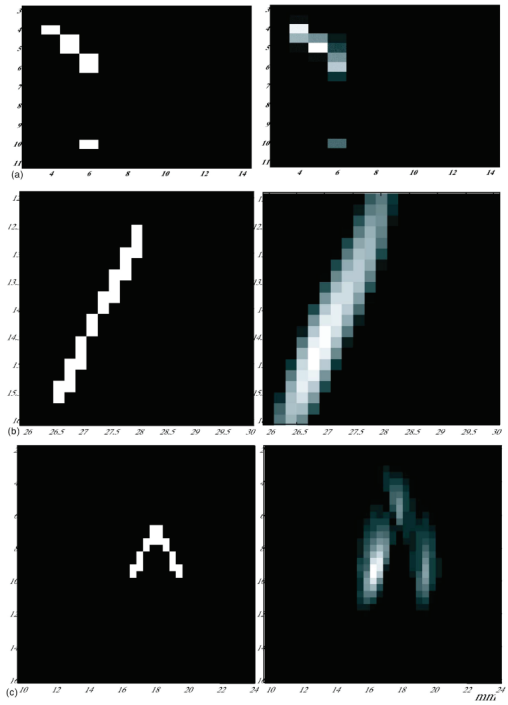

Simulation with multiple scatters (left column) and their reconstructions (right column). Distance from transducer a) 3-14 mm b) 10-24 mm c) 26-30 mm

- Object placed 4 mm apart and 17 mm distance from transducer
- The plot shows trend of increased distortion with higher sound speed. Corresponding error ranged from 4.3% at 1857 m/s to 13% at 3000 m/s
- Three scatterers placed diagonally in 8x8 ROI and additional object 4 mm apart
- Object as an inverted “V” was situated 18 mm from the ultrasound source.

Conclusion

- Large variation in image field makes it possible to localize the position of targets
- In numeric investigation objects where better defined and more spatially localized
- Small objects, which can be hard to detect, and even hard to localize using present methods may be both detected and localized.
- Only single receive channel was used.

Discussion

Thank you

Probabilistic Reconstruction in Compressed Sensing : Algorithms, Phase Diagrams, and Threshold Achieving Matrices

Authors: Florent Krzakala, Marc Mezard, Francois Sausset, Yifan Sun and Lenka Zdeborova

Publication: ArXiv:1206.3953v1 [Cond-mat.stat-mech] 18 Jun 2012

Speaker: Hyeong-ho, Baek

Short summary: In this paper, they present the probabilistic approach to reconstruction and discuss its optimality and robustness. And they detail the derivation of the message passing algorithm for reconstruction. Moreover, they further develop the asymptotic analysis of the corresponding phase diagrams with and without measurement noise, for different distribution of signals.

I. INTRODUCTION

The CS problem can be posed as follows: given an $N-$component signal $\mathbf{s}$, one makes M measurements that are grouped into an $M-$component vector $\mathbf{y}$, obtained from $\mathbf{s}$ by a linear transformation using $M \times N$ matrix $\mathbf{F}$, given by $y_\mu = \sum_{i=1}^{N} F_{\mu i} s_i$ with $\mu = 1, 2, ..., M$ .The aim is to reconstruct the signal $\mathbf{s}$ from the knowledge of $\mathbf{F}$ and $\mathbf{y}$. This amounts to inverting the linear system $\mathbf{y = Fs}$. However, we want to have M as small as possible and when $M < N$ there are fewer equations than unknowns. The system is under-determined and the inverse problem is ill-defined. However, CS deals with sparse signals. In the noiseless case, an exact reconstruction case, an exact reconstruction is possible for such signals as soon as $M > K$.

Candes, Tao, Donoho and collaborators proposed to find the vector satisfying the constraints $\mathbf{y = Fx}$ which has the smallest l_1 norm. This optimization problem is convex and can be solved using efficient linear programming techniques. For any signal with density $\rho = K / N$, the l_1 reconstruction gives indeed the exact result $\mathbf{x = s}$ with probability one only if

$\alpha = M/N > \alpha_{l_1}(\rho)$ is, however, larger than ρ. The l_1 reconstruction is thus sub-optimal: it requires more measurements than theoretically necessary.

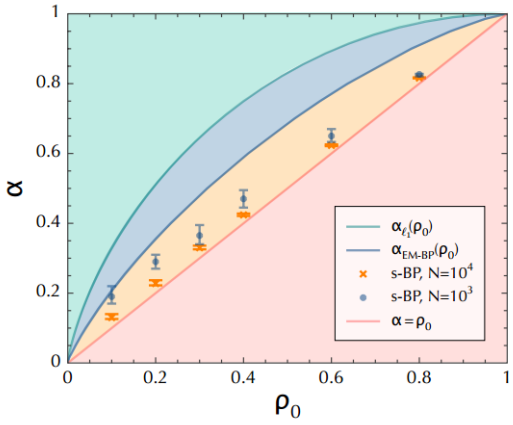

II. PROBABILISTIC RECONSTRUCTION IN COMPRESSED SENSING

The definition of the compressed sensing problem is as follows

$$y_\mu = \sum_{i=1}^{N} F_{ui} s_i + \xi_u \quad \mu = 1,...,M\,, \tag{1}$$

Where s_i are the signal elements, out of which only K are non-zero. F_{ui} are the elements of a known measurement matrix, y_μ are the known result of measurements, and ξ_u is Gaussian white noise on the measurement with variance Δ_μ. The goal of CS is to find an approach that allows reconstruction with as low values of α as possible.

We shall adopt a probabilistic inference approach to reconstruct the signal.

$$\hat{P}(\mathbf{x}) = \frac{1}{Z}\prod_{i=1}^{N}[(1-\rho)\delta(x_i) + \rho\phi(x_i)]\prod_{\mu=1}^{M}\frac{1}{\sqrt{2\pi\Delta_\mu}} e^{-\frac{1}{2\Delta_\mu}(y_\mu - \sum_{i=1}^{N} F_{\mu i} x_i)^2}\,, \tag{2}$$

Where Z, the partition function, is a normalization constant. Here we model the signal as stochastic with iid entries, the fraction of non-zero entries being $\rho > 0$ and their distribution being ϕ.

We stress that in general the signal properties are not known and hence we do not assume that the signal model matches the empirical signal distribution, $\rho = \rho_0, \Delta = \Delta_0, \phi = \phi_0$. One crucial point in our approach is using $\rho < 1$ which includes the fact that on searches a sparse signal in the model of the signal.

A. The Bayesian optimality and the Nishimori condition

The probabilistic approach can also be recovered from a Bayesian point of view. Indeed, given $\mathbf{F}$ and $\mathbf{y}$, from Bayes theorem, we have

$$P(\mathbf{x}\,|\,\mathbf{F},\mathbf{y}) = \frac{P(\mathbf{x}\,|\,\mathbf{F})P(\mathbf{y}\,|\,\mathbf{F},\mathbf{x})}{P(\mathbf{y}\,|\,\mathbf{F})} \tag{3}$$

The value of measurements $\mathbf{y}$ given the knowledge of the matrix $\mathbf{F}$ and the signal $\mathbf{x}$ is, by definition of the problem, given by $P(\mathbf{y}\,|\,\mathbf{F},\mathbf{x}) = \prod_{\mu=1}^{M} \delta(y_\mu - \sum_{i=1}^{N} F_{\mu i} x_i)$ in the noiseless case, and by

$$P(y\,|\,F,x) = \prod_{\mu=1}^{M} \frac{1}{\sqrt{2\pi\Delta_\mu}} e^{-\frac{1}{2\Delta_\mu}(y_\mu - \sum_{i=1}^{N} F_{\mu i} x_i)^2} \tag{4}$$

With random Gaussian measurement noise of variance Δ_μ, for measurement μ. To express the probability $P(\mathbf{x}\,|\,\mathbf{F})$ we consider that the signal dose not depend on the measurement matrix. And we model the signal as an iid:

$$P(x\,|\,F) = \prod_{i=1}^{N} \left[(1-\rho)\delta(x_i) + \rho\phi(x_i) \right] \tag{5}$$

Thus the posterior probability of $\mathbf{x}$ after the measurement of $\mathbf{y}$ is given by

$$P(\mathbf{x}\,|\,\mathbf{F},\mathbf{y}) = \frac{1}{Z(\mathbf{y},\mathbf{F})}\prod_{i=1}^{N}\left[(1-\rho)\delta(x_i)+\rho\phi(x_i)\right]\prod_{\mu=1}^{M}\frac{1}{\sqrt{2\pi\Delta_\mu}}e^{-\frac{1}{2\Delta_\mu}(y_\mu-\sum_{i=1}^{N}F_{\mu i}x_i)^2}, \tag{6}$$

Where $Z(\mathbf{y},\mathbf{F}) = P(\mathbf{y}\,|\,\mathbf{F})$ is again the normalization constant.

An estimator $\mathbf{x}^*$ that minimizes mean-squared error with respect to the original signal $\mathbf{s}$, defined as $E = \sum_{i=1}^{N}(x_i - s_i)^2 / N$, is then obtained from averages of x_i with respect to the probability measure $P(\mathbf{x}\,|\,\mathbf{F},\mathbf{y})$, i.e.,

$$x_i^* = \int dx_i x_i v_i(x_i), \tag{7}$$

Where $v_i(x_i)$ is the marginal probability distribution of the variable i

$$v_i(x_i) \equiv \int_{\{x_j\}_{j\neq i}} P(\mathbf{x}\,|\,\mathbf{F},\mathbf{y}). \tag{8}$$

III. THE BELIEF PROPAGATION RECONSTRUCTION ALGORITHM FOR COMPRESSED SENSING

Exact computation of the averages $x_i^* = \int dx_i x_i v_i(x_i)$ requires exponential time and is thus intractable. To approximate the expectations we will use a variant of the belief propagation(BP) algorithm. Indeed, message passing has been shown very efficient in terms of both precision and speed for the CS problem.

A. Belief Propagation recursion

The canonical BP equation for the probability measure $P(\mathbf{x}\,|\,\mathbf{F},\mathbf{y})$ are expressed in terms of $2MN$ "messages", $m_{\mu\to j}(x_j)$ and $m_{j\to\mu}(x_j)$, which are probability distribution functions.

$$m_{\mu\to i}(x_i)=\frac{1}{Z^{\mu\to i}}\int\prod_{j\neq i}dx_j e^{-\frac{1}{2\Delta_\mu}\left(\sum_{j\neq i}F_{\mu j}x_j+F_{\mu i}x_i-y_\mu\right)^2}\prod_{j\neq i}m_{j\to\mu}(x_j), \tag{9}$$

$$m_{i\to\mu}(x_i)=\frac{1}{Z^{i\to\mu}}\left[(1-\rho\delta(x_i)+\rho\phi(x_i)\right]\prod_{\gamma\neq\mu}m_{\gamma\to i}(x_i), \tag{10}$$

Where $Z^{\mu\to i}$ and $Z^{i\to\mu}$ are normalization factors ensuring that $\int dx_i m_{\mu\to i}(x_i)=1$, $\int dx_i m_{i\to\mu}(x_i)=1.$

Using the Hubbard-Stratonovich transformation

$$e^{-\frac{w^2}{2\Delta}}=\frac{1}{\sqrt{2\pi\Delta}}\int d\lambda e^{-\frac{\lambda^2}{2\Delta}+\frac{i\lambda w}{\Delta}} \tag{11}$$

For $w=\left(\sum_{j\neq i}F_{\mu j}x_j\right)$ we can simplify Eq.(9) as

$$m_{\mu\to i}(x_i)=\frac{1}{Z^{\mu\to i}\sqrt{2\pi\Delta}}e^{-\frac{1}{2\Delta_\mu}(F_{\mu i}x_i-y_\mu)^2}\int d\lambda e^{-\frac{1}{2\Delta_\mu}}\prod_{j\neq i}\left[\int dx_j m_{j\to\mu}(x_j)e^{\frac{F_{\mu j}x_j}{\Delta_\mu}(y_\mu-F_{\mu i}x_i+i\lambda)}\right] \tag{12}$$

The integration over scalar x_j takes the form of the moment generating function. Therefore,

$$m_{\mu\to i}(x_i)=\frac{1}{Z^{\mu\to i}\sqrt{2\pi\Delta}}e^{-\frac{1}{2\Delta_\mu}(F_{\mu i}x_i-y_\mu)^2}\int d\lambda e^{-\frac{\lambda^2}{2\Delta_\mu}}\prod_{j\neq i}E_{X_j}\left[e^{\frac{F_{\mu j}x_j}{\Delta_\mu}(y_\mu-F_{\mu i}x_i+i\lambda)}\right] \tag{13}$$

By assuming that each scalar X_j is Gaussian distributed, the moment generating function is expressed using means and variance. Thus, introducing means and variances as “messages”

$$a_{i\to\mu}\equiv\int dx_i x_i m_{i\to\mu}(x_i), \tag{14}$$

$$v_{i\to\mu}\equiv\int dx_i x_i^2 m_{i\to\mu}(x_i)-a_{i\to\mu}^2 \tag{15}$$

We obtain

$$m_{\mu\to i}(x_i)=\frac{1}{Z^{\mu\to i}\sqrt{2\pi\Delta}}e^{-\frac{1}{2\Delta_\mu}(F_{\mu i}x_i-y_\mu)^2}\int d\lambda e^{-\frac{\lambda^2}{2\Delta_\mu}}\prod_{j\neq i}\left[e^{\frac{F_{\mu j}a_{j\to\mu}}{\Delta_\mu}(y_\mu-F_{\mu i}x_i+i\lambda)+\frac{F_{\mu j}^2 v_{j\to\mu}}{2\Delta_\mu^2}(y_\mu-F_{\mu i}x_i+i\lambda)}\right] \tag{16}$$

Performing the Gaussian integral over λ, we obtain

$$m_{\mu\to i}(x_i)=\frac{1}{\widetilde{Z}^{\mu\to i}}e^{-\frac{x_i^2}{2}A_{\mu\to i}+B_{\mu\to i}x_i},\quad \widetilde{Z}^{\mu\to i}=\sqrt{\frac{2\pi}{A_{\mu\to i}}}e^{\frac{B_{\mu\to i}^2}{2A_{\mu\to i}}} \tag{17}$$

Where

$$A_{\mu\to i}=\frac{F_{\mu i}^2}{\Delta_\mu+\sum_{j\neq i}F_{\mu j}^2 v_{j\to\mu}} \tag{18}$$

$$B_{\mu\to i}=\frac{F_{\mu i}(y_\mu-\sum_{j\neq i}F_{\mu j}a_{j\to\mu})}{\Delta_\mu+\sum_{j\neq i}F_{\mu j}^2 v_{j\to\mu}} \tag{19}$$

To close the equation on messages $a_{i\to\mu}$ and $v_{i\to\mu}$ we notice that

$$m_{i\to\mu}(x_i)=\frac{1}{\widetilde{Z}^{i\to\mu}}[(1-\rho)\delta(x_i)+\rho\phi(x_i)]e^{-\frac{x_i^2}{2}\sum_{\gamma\neq\mu}A_{\gamma\to i}+x_i\sum_{\gamma\neq\mu}B_{\gamma\to i}} \tag{20}$$

Message $a_{i\to\mu}$ and $v_{i\to\mu}$ are respectively the mean and variance of the probability distribution $m_{i\to\mu}(x_i)$. It also useful to define the local beliefs a_i and v_i as

$$a_i\equiv\int dx_i x_i m_i(x_i) \tag{21}$$

$$v_i\equiv\int dx_i x_i^2 m_i(x_i)-a_i^2, \tag{22}$$

Where

$$m_i\left(x_i\right)=\frac{1}{\widetilde{Z}^i}[(1-\rho)\delta(x_i)+\rho\phi(x_i)]e^{-\frac{x_i^2}{2}\sum_\gamma A_{\gamma\to i}+x_i\sum_\gamma B_{\gamma\to i}} \tag{23}$$

Let us define the probability distribution

$$\mathrm{M}_\phi\left(\sum{}^2,R,x\right)=\frac{1}{\widehat{Z}(\sum{}^2,R)}[(1-\rho)\delta(x)+\rho\phi(x)]\frac{1}{\sqrt{2\pi\sum}}e^{-\frac{(x-R)^2}{2\sum{}^2}}, \tag{24}$$

$$\sum{}^2:=\frac{1}{\sum_{\gamma\neq\mu}A_{\gamma\to i}},\quad R:=\frac{\sum_{\gamma\neq\mu}B_{\gamma\to i}}{\sum_{\gamma\neq\mu}A_{\gamma\to i}}$$

Where $\widehat{Z}(\sum{}^2,R,x)$ is normalization. We define the average and variance of M_ϕ as

$$f_a(\sum{}^2,R)\equiv\int dx x\mathrm{M}(\sum{}^2,R,x) \tag{25}$$

$$f_c(\sum{}^2,R)\equiv\int dx x^2\mathrm{M}(\sum{}^2,R,x)-f_a^2(\sum{}^2,R) \tag{26}$$

The closed form of the BP update is

$$a_{i\to\mu}=f_a\left(\frac{1}{\sum_{\gamma\neq\mu}A_{\gamma\to i}},\frac{\sum_{\gamma\neq\mu}B_{\gamma\to i}}{\sum_{\gamma\neq\mu}A_{\gamma\to i}}\right),\quad a_i=f_a\left(\frac{1}{\sum_\gamma A_{\gamma\to i}},\frac{\sum_\gamma B_{\gamma\to i}}{\sum_\gamma A_{\gamma\to i}}\right), \tag{27}$$

$$v_{i\to\mu}=f_c\left(\frac{1}{\sum_{\gamma\neq\mu}A_{\gamma\to i}},\frac{\sum_{\gamma\neq\mu}B_{\gamma\to i}}{\sum_{\gamma\neq\mu}A_{\gamma\to i}}\right),\quad v_i=f_c\left(\frac{1}{\sum_\gamma A_{\gamma\to i}},\frac{\sum_\gamma B_{\gamma\to i}}{\sum_\gamma A_{\gamma\to i}}\right) \tag{28}$$

For a general signal model $\phi(x_i)$ the functions f_a and f_c can be computed using a numerical integration over x_i. Eqs. (14-15) together with (18-19) and (20) lead to closed iterative message passing equation, which can be solved by iterations. There equation can be used for any signal $\mathbf{s}$, and any matrix $\mathbf{F}$. When a fixed point of the BP equations is reached, the

elements of the original signal are estimated as $x_i^* = a_i$, and the corresponding variance v_i can be used to quantify the correctness of the estimate. Perfect reconstruction is found when the message converge to a fixed point such that $a_i = s_i$ and $v_i = 0$.

IV. DISCUSSION

After meeting, please write discussion in the meeting and update your presentation file.

Reference

[1] Krzakala F., Mezard M., Sausset F., Sun Y. & Zdeborova L. Statistical physics-based reconstruction in compressed sensing. Phys. Rev. X 021005 (2012).

[2] Candes E. J. & Wakin M. B. An Introduction To Compressive Sampling. IEEE Signal Processing Magazine 25, 21-30 (2008).

[3] Donoho D., Maleki A. & Montanari A. Message passing algorithms for compressed sensing: I. motivation and construction. In Information Theory Workshop (ITW), 2010 IEEE, 1 {5 (2010).

[4] Donoho D. L., Javanmard A. & Montanari A. Information-Theoretically Optimal Compressed Sensing via Spatial Coupling and Approximate Message Passing (2011). ArXiv:1112.0708v1 [cs.IT]

[5] Montanari A. & Bayati M. Message-passing algorithms for compressed sensingThe dynamics of message passing on dense graphs, with applications to compressed sensing (2010). ArXiv:1001.3448.

[6] Rangan S. Estimation with random linear mixing, belief propagation and compressed sensing. In Information Sciences and Systems (CISS), 2010 44th Annual Conference on, 1-6 (2010).

[7] Montanari A. & Bayati M. Message-passing algorithms for compressed sensingThe dynamics of message passing on dense graphs, with applications to compressed sensing (2010). ArXiv:1001.3448

[8] Bayati M., Lelarge M. & Montanari A. Universality in message passing algorithms (2012). In preparation.

[9] Wu Y. & Verdu S. Renyi information dimension: fundamental limits of almost lossless analog compression. IEEE Transactions on Information Theory 56, 37213747 (2010).

[10] Wu Y. & Verdu S. Optimal Phase Transitions in Compressed Sensing (2011). ArXiv:1111.6822v1 [cs.IT].

[11] Wu Y. & Verdu S. MMSE Dimension. IEEE Transactions on Information Theory 57, 4857 - 4879 (2011).

[12] Baron D., Sarvotham S. & Baraniuk R. Bayesian Compressive Sensing Via Belief Propagation. IEEE Transactions on Signal Processing 58, 269 - 280 (2010).

[13] Rangan S., Fletcher A. & Goyal V. Asymptotic Analysis of MAP Estimation via the Replica Method and Applications to Compressed Sensing. arXiv:0906.3234v2 (2009).

[14] Donoho D. L., Johnstone I. & Montanari A. Accurate Prediction of Phase Transitions in Compressed Sensing via a Connection to Minimax Denoising (2011). ArXiv:1111.1041v1 [cs.IT].

DASHER - An Efficient Writing System for Brain Computer Interfaces?

Sebastian A. Wills and David J. C. MacKay

IEEE Trans. Neural systems and Rehabilitation Engineering. (2006.06)

Presenter : Soogil Woo
GIST, Dept. of Information and Communication, INFONET Lab.

Gwangju Institute of Science and Technology

Background

- The P300 (P3) wave is an event related potential (ERP) component elicited in the process of decision making.
- In neurology, Steady State Visually Evoked Potentials (SSVEP) are signals that are natural responses to visual stimulation at specific frequencies. When the retina is excited by a visual stimulus ranging from 3.5 Hz to 75 Hz, the brain generates electrical activity at the same (or multiples of) frequency of the visual stimulus.
- Dasher is a computer accessibility tool which enables users to write without using a keyboard, by entering text on a screen using a pointing device such as a mouse, a touchpad, a touch screen, a roller ball, a joystick, a Push-button, or even mice operated by the foot or head.

Introduction

- DASHER is a human computer interface for entering text using continuous or discrete gestures.
- DASHER efficiently converts bits received from the user into text, and has been shown to be a competitive alternative to existing text-entry methods in situations where an ordinary keyboard cannot be used. (PDAs, mobile phones, for handicapped person)
- DASHER is free, open-source software.
- In DASHER, the size of each box within its parent box is determined by the corresponding letter's probability according to a language model.
- As result, sequences of characters that are well predicted by the language model take less time to zoom into.
- Improbable sequences of characters are always possible to write, but take longer.

Introduction & Overall Users' View

- They first describe how Dasher is used to enter the word 'the'.
- Figure (a) show the initial configuration, with an alphabet of 27 characters displayed in a column.
- There are 26 lower case letters and the symbol '_'(under bar) represents a space.
- The user writes the first letter by making a gesture towards the letter's rectangle.
- The trails show the user moving the mouse towards the letter 't'.

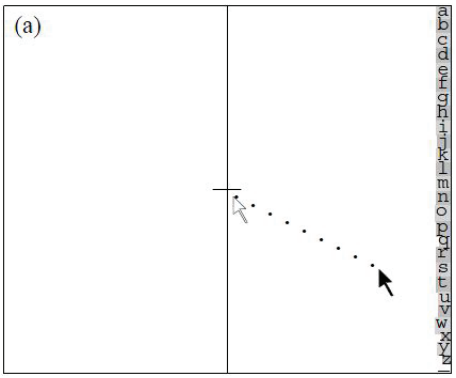

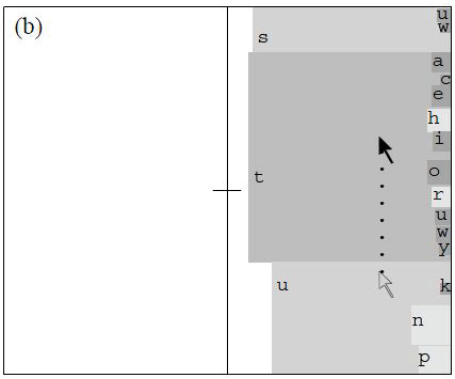

Introduction & Overall Users' View

- The point of view zooms towards this letter (figure (b)).
- As the rectangles get larger possible extensions of the written string appear within the rectangle that they are moving towards.
- If they are moving into the 't', rectangles corresponding to 'ta', 'tb',…, 'th',…,'tz' appear in a vertical line like the first line.
- The heights of the rectangles correspond to the probabilities of these strings, given the languages.

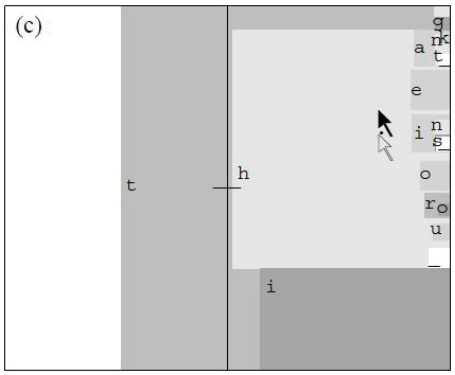

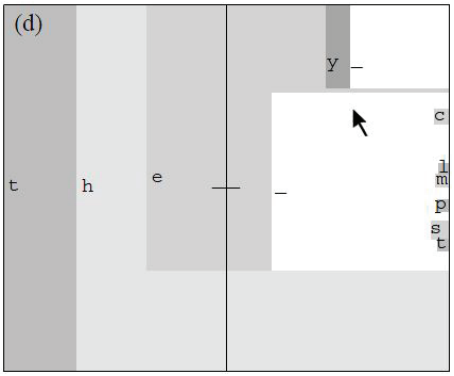

Introduction & Overall Users' View

- In English, 'ta' is quite probable; 'tb', is less so; 'th' is very probable.
- It is easy to gesture our point of view into 'th' (figure (c)), and from there into 'the' (figure (d)).

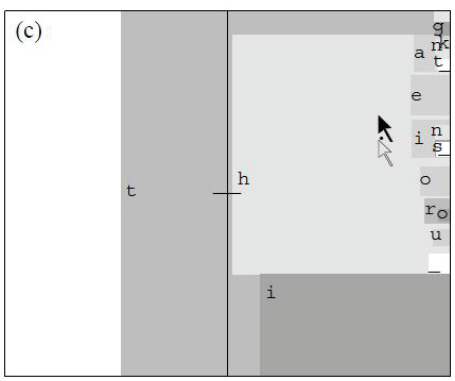

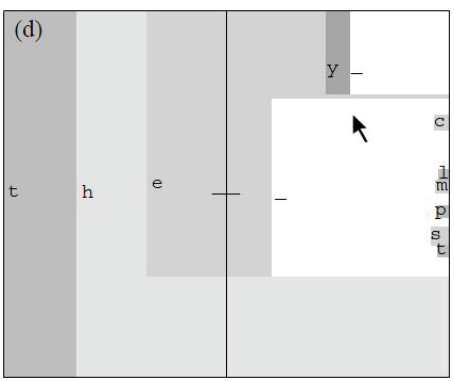

Introduction & Probabilistic Model Determines

- In a given context, they display the alphabet of possible continuations as a column of characters as shown in figure 2.
- The division of the right-hand vertical is analogous to arithmetic coding.
- Let their alphabet be $A_X = \{a_1, a_2, ..., a_I\}$.
- They divide the real line[0,1) into I intervals of lengths equal to the probabilities $P(x_i = a_i)$.
- They subdivide the interval a_i into intervals denoted $a_i a_1, a_i a_2, a_i a_3, ..., a_i a_I$ such that the length of the interval $a_i a_j$ is

$$P(x_1 = a_1, x_2 = a_2) = P(x_1 = a_i) P(x_2 = a_j \mid x_1 = a_i)$$

- They use a language model. (PPM and PPM5D+)

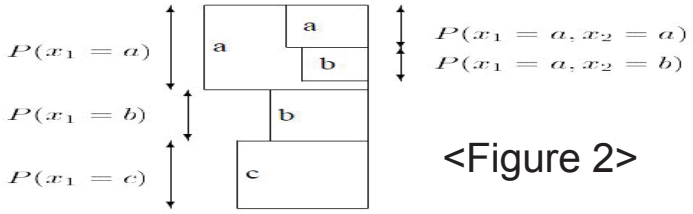

<Figure 2>

Input Devices currently used with DASHER

A. 2-D Continuous Input

- DASHER was first developed to be driven by continuous two-dimensional (2-D) gestures by directly controlling the position of a pointer on the screen.
- If the user moves the pointer away from the origin, the interface zooms in towards the location pointed to by the vector from the origin to the pointer.
- 2-D input devices used with DASHER include mouse, touch-screen, gaze tracker, and head mouse.
- Under mouse control, novice users can reach writing speeds of 25 words/min after 1 h of practice; expert users can write at 35 words/min.
- Under eye control alone users familiar with DASHER can write at 25 words/min, faster than any other gaze-writing system they are aware of.

Input Devices currently used with DASHER

A. 2-D Continuous Input (Example)

Input Devices currently used with DASHER

B. 1-D Continuous Input

- For input devices offering a single continuous dimension of control, DASHER maps the one-dimensional (1-D) input onto a continuous curve within the normal 2-D control space.
- Midrange values of the input control the direction in which to zoom.
- Values towards the extremes of the available range allow the user to zoom out and pause the interface.

C. Discrete Inputs

- Users who can activate buttons (virtual or physical) but cannot reliably provide a continuous output can use one of DASHER's "button modes". (The direct 2-button mode maps 1 button to the action of zooming in one the top half of the visible DASHER land-scape, and the second button to zooming in on the bottom half.)

Input Devices currently used with DASHER

C. Discrete Inputs

- In button mode, DASHER converts bits from the user into written text at exactly the compression rate achieved by the language model.
- DASHER's current language model PPMD5 compresses English text to around 2 bits per character.
- DASHER outputs one character for every two bits provided by the user's button presses.

DASHER as a BCI user interface

A. Motivation

- Current brain computer interface (BCI) systems extract data from the user at a lower information transfer rate than typical physical user interfaces.
- DASHER offers an efficient method for converting the output of a BCI into text.
- DASHER can also use information about the reliability if the signals generated by the user.
- DASHER's language model can be initialized using text that is biased towards a limited set of phrases and words that the user is likely to wish to communicate.
- The user will be able to write these phrases, or variants of them, extremely quickly, while retaining the ability to write any other phrase should they wish to.

DASHER as a BCI user interface

B. Continuous Control

- Many BCI systems output a continuous 1- or 2-D signal which could be used to drive DASHER directly.
- DASHER is well-suited to a BCI signal which is likely to be under imperfect control of the user.
- In DASHER, users write by navigating to what they want to say, not by selecting letters or words.
- If the user accidentally steers in the wrong direction, they can correct their mistake by subsequent compensatory action.
- As with all navigation, all that matters is the final location arrived at.

DASHER as a BCI user interface

C. Discrete Control

- BCI systems that emit discrete events fall into two categories.
- The first category contains systems which internally convert a continuous variable into discrete outputs
- Systems in which the user makes selections by driving a cursor to one of two or more on-screen targets fall into this category.
- They suggest that the best strategy for using DASHER with BCI systems in this category may be to use the continuous variable to drive DASHER directly, without an intermediate conversion into discrete options.
- The second category contains systems which are intrinsically discrete in nature.
- For example, both P300 and steady-state visually evoked potential (SSVEP) interfaces determine which of several discrete visual targets the user is attending to.

DASHER as a BCI user interface

C. Discrete Control

- A natural way to use these techniques would be to paint P300 targets or SSVEP regions onto the DASHER landscape.
- For example, in the case of SSVEP, the right-hand half of the DASHER landscape could be covered by two or more regions flickering at different frequencies (Fig. 3).

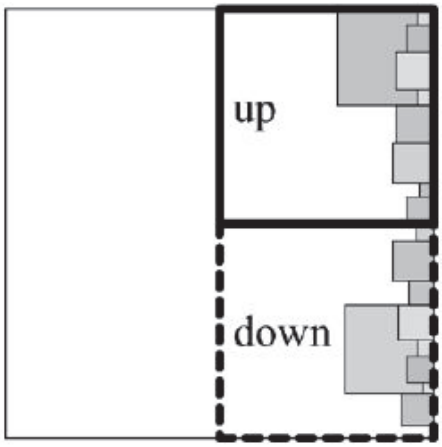

Depending on which region the user attends to, DASHER zooms in on the top or bottom half of the screen. <Figure 3>

DASHER as a BCI user interface

C. Discrete Control

- To zoom into one of these regions, the user attends to that region.
- The BCI system detects which region the user is attending to and causes DASHER to zoom in appropriately, and the cycle repeats. Likewise, P300 targets could be arranged down the right-hand side of the DASHER landscape, instead of in the commonly used speller grid.
- If the accuracy of the BCI system is high, then the optimal strategy for dealing with the rare errors that do occur may be to simply provide an additional target which instructs DASHER to undo the previous action (i.e., zoom out).
- Such a target needs to be present anyway, in case the user makes a mistake in selecting which region of the DASHER landscape contains the text they are trying to write.
- This is similar to the strategy of adding a “delete” node to a binary decision tree.

DASHER as a BCI user interface

C. Discrete Control

- However, if the BCI misclassification rate is high, they suggest that the optimal strategy is to model the BCI system as a noisy communication channel between the user and the computer, and to use information theory to inform the choice of an error-correcting code to use.
- For example, instead of accumulating evidence that the user is attending to a particular target over a single, long trial, it may be more efficient to run several shorter trials, each one individually less reliable.
- By varying the SSVEP frequencies on each target in each trial according to the coding scheme specied by the error-correcting code, the overall information transfer rate may be improved.

Conclusion

- They wish to make the best possible use of the bits of information content that can be generated by severely disabled people.
- DASHER offers a paradigm for efficiently converting these bits to communication symbols.
- DASHER has proved its effectiveness for people able to use a gaze tracker or make other motor actions.
- DASHER will be equally useful to users who retain functioning vision but are limited to communication through a BCI.

Idea

- DASHER + SSVEP (Continuous Control) (Mouse Control)

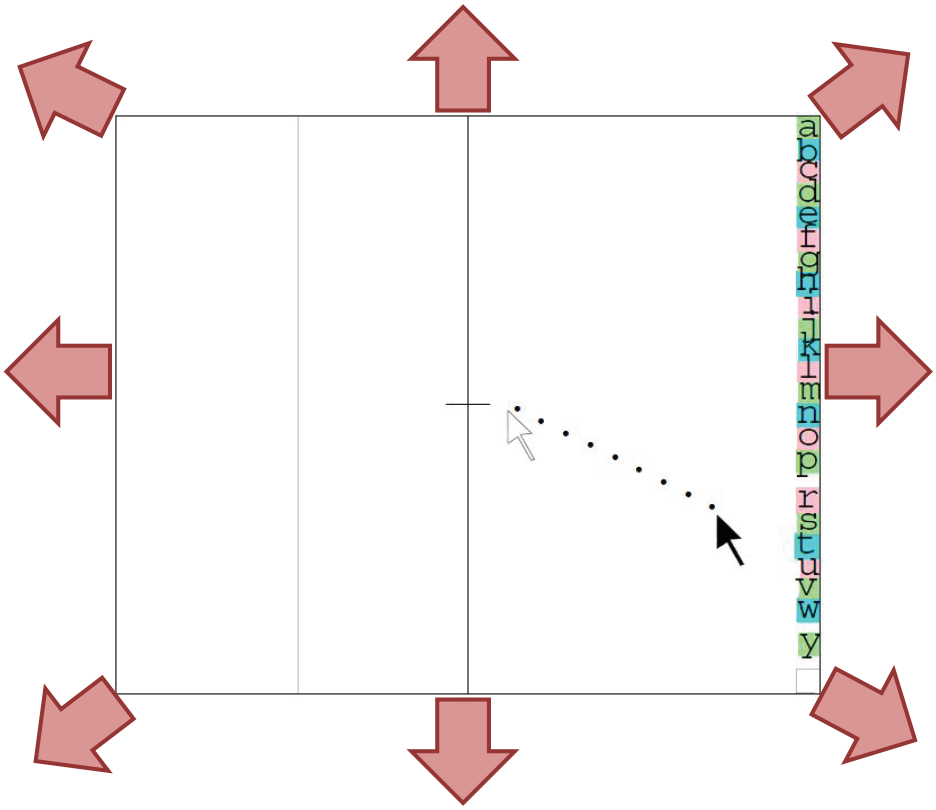

Thank you!

Title: Speckle field digital holographic microscopy

Wonshik Choi, YongKeun Park, Zahid Yaqoob, Ramachandra Dasari, Kamran Badizadegan, and Michael S. Feld

Speaker: Nitin Rawat

Brief Summary:

I. General Overview.

II. Experimental setup

III. Hologram reconstruction

This material is presented at the INFONT's Compressive Sensing Seminar

Lab Homepage: http://infonet.gist.ac.kr

Seminar Homepage: http://infonet.gist.ac.kr/twiki/bin/view/Main/CompressiveSensing

Advisor: Prof. Heung-no Lee

Speckle-field digital holographic microscopy

Conventional Holographic phase microscopy (HPM) uses a plane wave illumination that has very limited aperture in a condenser lens. This leads to poor spatial resolution compared with diffraction-limited resolution of conventional bright field microscopy.

Speckle field digital holographic microscopy (SFDHM), an interferometry-based light microscopic technique for sensing complex electric field (E-field) which utilizes the speckle field for illumination.

Principle

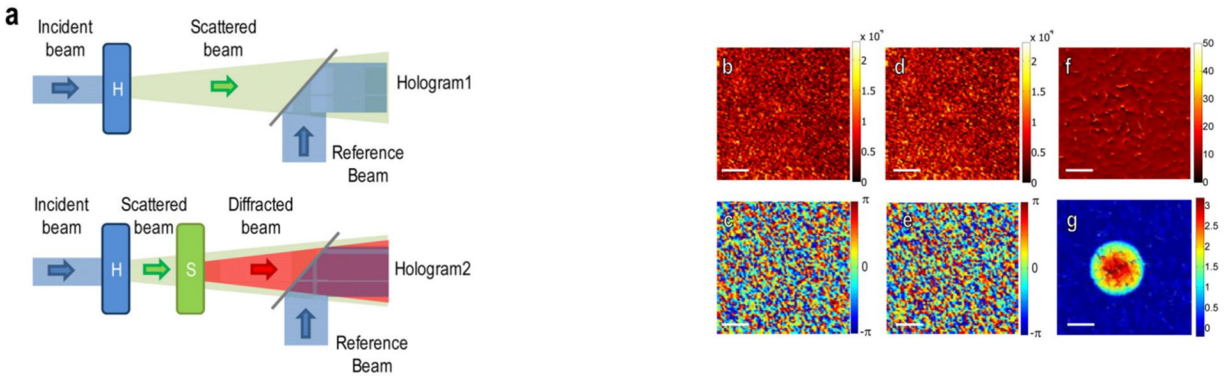

Figure. 1

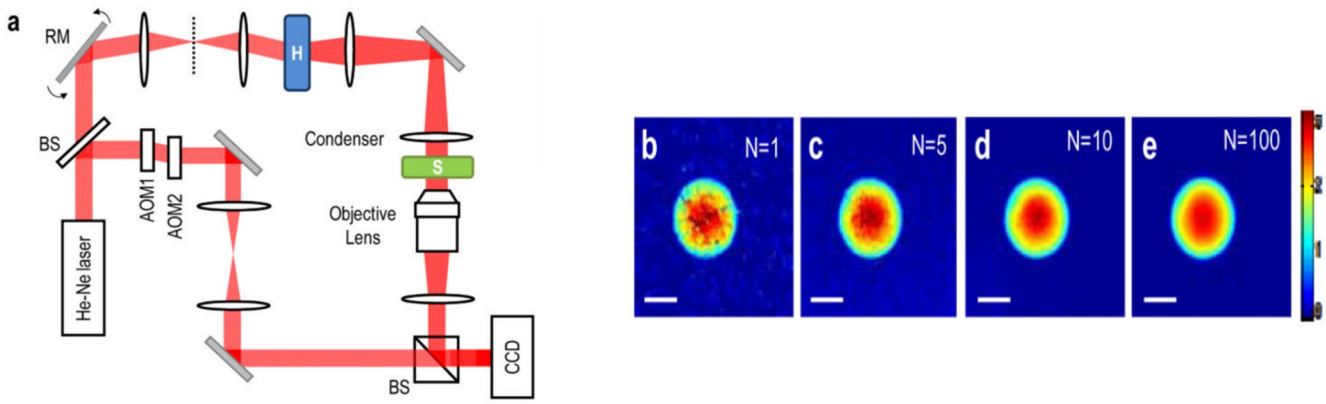

Figure.2

They generated a speckle field by illuminating a holographic diffuser with a He-Ne laser. The speckle field traveled through a microscope and was imaged on a detector. The hologram of the speckle field was generated by imposing a plane-wave reference beam on the detector. Using a heterodyne Mach-Zehnder interferometer, a complex E-field of the speckle was retrieved, as shown in figure 1b-c.

Then a sample was inserted on the sample stage with the same speckle field illumination. Introducing the sample modified the original speckle pattern.

Next, the E-field of the modified speckle was recorded in the same way as the recording of the original speckle pattern (Figs. 1d-e). The sample is almost invisible in these images since its image is overlapped with the complex pattern of the speckle field.

The background speckle field can be removed and the sample-induced complex field image can be retrieved from the speckle field (Fig. 1b-c) by dividing it by the field without the sample (Fig. 1d-e).

As a result, the sample becomes clearly visible, as shown in figs. 1f-g.

Speckle illumination not only reduces diffraction noise but also enhances the resolution in comparison with conventional HPM.

Holographic process

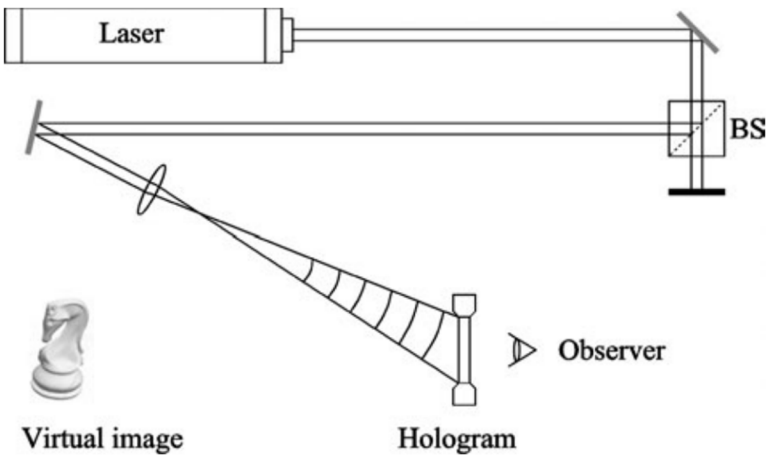

Light with sufficient coherence length is split into two partial waves by a beam splitter (BS). One wave illuminates the object, is scattered and reflected to the recording medium, e.g. a photographic plate.

The second wave, called the reference wave, illuminates the plate directly. Both waves are interfering. The recorded interference pattern is called hologram.

The holographic process is described mathematically as follows:

$$O(x,y) = o(x,y)\exp(i\varphi_o(x,y)) \quad \text{... (1.1)}$$

Is the complex amplitude of the object wave with real amplitude o and phase φ_o and

$$R(x,y) = r(x,y)\exp(i\varphi_R(x,y)) \quad \text{... (1.2)}$$

Is the complex amplitude of the reference wave with real amplitude r and phase φ_R

Both waves interfere at the surface of the recording medium (CCD). The intensity is calculated by

$$I(x,y) = \left|O(x,y) + R(x,y)\right|^2$$

$$= (O(x,y) + R(x,y))(O(x,y) + R(x,y))^*$$

$$= R(x,y)R^*(x,y) + O(x,y)O^*(x,y)$$

$$+ O(x,y)R^*(x,y) + R(x,y)O^*(x,y) \quad \text{... (1.3)}$$

Where $*$ denotes the conjugate complex.

The amplitude transmission *h(x,y)* of the developed photographic plate (or CCD) is proportional to *I(x,y)* :

$$h(x,y) = h_o + \beta\tau I(x,y) \quad \text{... (1.4)}$$

Where β is a constant, τ is the exposure time and h_o is the amplitude transmission of the unexposed plate. $h(x,y)$ is also called the hologram function.

In digital holography using CCD's as recording medium h_o can be neglected.

For hologram reconstruction the amplitude transmission has to be multiplied with the complex amplitude of the reconstruction (reference) wave:

$$R(x,y)h(x,y) = [h_o + \beta\tau(r^2 + o^2)]R(x,y) + \beta\tau r^2 O(x,y) + \beta\tau R^2(x,y)O^*(x,y) \quad \text{... (1.5)}$$

$$R(x,y)h(x,y) = \underbrace{[h_o + \beta\tau(r^2 + o^2)]R(x,y)}_{\text{reference wave multiplied by a factor}} + \underbrace{\beta\tau r^2 O(x,y)}_{\text{reconstructed object wave, forming the virtual image}} + \underbrace{\beta\tau R^2(x,y)O^*(x,y)}_{\text{distorted real image of the object}}$$

The first term on the right side of this equation is the reference wave, multiplied by a factor. It represents the un-diffracted wave passing through the hologram (zero diffraction order).

The second term is the reconstructed object wave, forming the virtual image. The factor $\beta\tau r^2$ only influences the brightness of the image.

The third term produces a distorted real image of the object.

For off-axis holography the virtual image, the real image and the un-diffracted wave are spatially separated.

Optical Path change

The hologram is reconstructed by illumination with the reference wave. As a result of the superposition of the two holographic recordings with slightly different object waves only one image superimposed by interference fringes is reconstructed.

The complex amplitude of the object wave in the initial state is

$$O_1(x,y) = o(x,y)\exp[i\varphi(x,y)] \quad \text{... (1.6)}$$

Where $o(x,y)$ is the real amplitude and $\varphi(x,y)$ is the phase of the object wave.

Optical path changes due to deformations of the object surface can be described by a variation of the phase from $\varphi \; to \; \varphi + \Delta\varphi$. $\Delta\varphi$ is the difference between the initial and actual phase, and is called the *interference phase*. The complex amplitude of the actual object wave is therefore denoted by:

$$O_2(x,y) = o(x,y)\exp[i(\varphi(x,y) + \Delta\varphi(x,y))] \quad \text{... (1.7)}$$

The intensity of a holographic interference pattern is described by the square of the sum of the complex amplitudes. It is calculated as follows:

$$I(x,y) = |O_1 + O_2|^2 = (O_1 + O_2)(O_1 + O_2)^* \quad \text{... (1.8)}$$

Equation (1.8) describes the relation between the intensity of the interference pattern and the interference phase, which contains the information about the deformation.

Several techniques have been developed to determine the interference phase by recording additional information. The most commonly used techniques are the various phase-shifting methods.

The interference phase is the key to calculate quantities representing the object under investigation. These are the displacement vector field of the surface in the case of opaque bodies.

The interference phase is the key to calculate quantities representing the object under investigation. These are the displacement vector field of the surface in the case of opaque bodies or refractive index changes within transparent media.

Yet to explore

General Principles

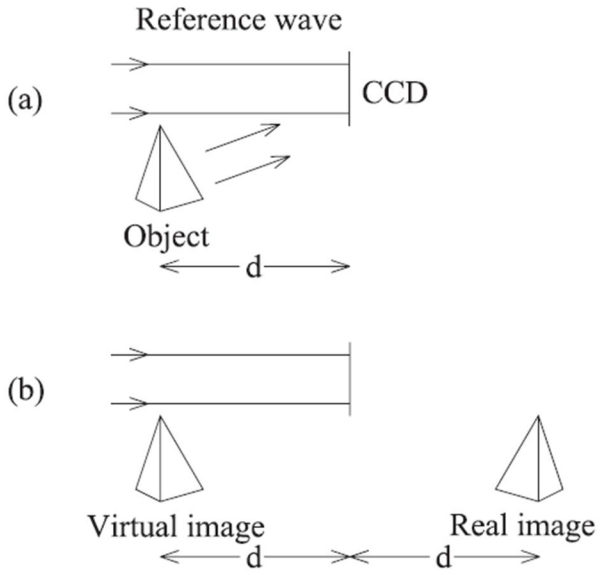

A general set-up for digital recording of off-axis holograms is shown in above above figure. A plane reference wave and the wave reflected from the object are interfering at the surface of a CCD. The resulting hologram is electronically recorded and stored.

The object is, in general, a three-dimensional body with diffusely reflecting surface, located at a distance *d* from the CCD.

In optical reconstruction the virtual image appears at the position of the original object and the real image is formed also at a distance *d*, but in the opposite direction from the CCD, see figure (b).

The diffraction of a light wave at an aperture (in this case a hologram) which is fastened perpendicular to the incoming beam is described by the Fresnel-Kirchhoff integral

$$\Gamma(\xi,\eta)=\frac{i}{\lambda}\int_{-\infty}^{\infty}\int_{-\infty}^{\infty}h(x,y)R(x,y)\frac{\exp(-i\frac{2\pi}{\lambda}\rho)}{\rho}\times(\frac{1}{2}+\frac{1}{2}\cos\theta)dx\,dy \quad \text{... (2.1)}$$

With $\rho=\sqrt{(x-\xi)^2+(y-\eta)^2+d^2}$ ... (2.2)

Where $h(x,y)$ is again the hologram function and ρ is the distance between a point in the hologram plane and a point in the reconstruction plane, see figure 5.

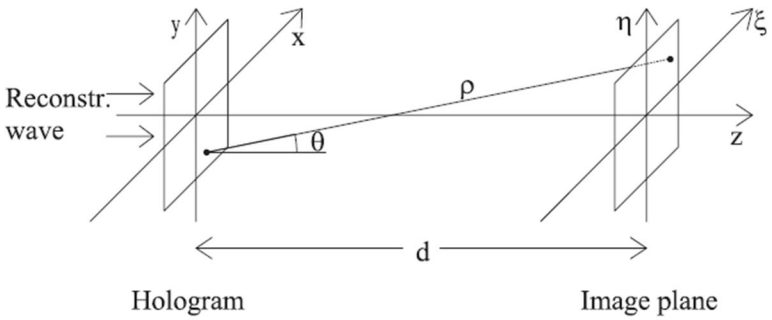

For a plane reference wave $R(x, y)$ is simply given by the real amplitude:

$$R = r + i0 = r \qquad \text{... (2.3)}$$

The diffraction pattern is calculated at a distance *d* behind the CCD plane, which means it reconstructs the complex amplitude in the plane of the real image.

Equation (2.2) is the basis for numerical hologram reconstruction. Because the reconstructed wave-field $\Gamma(\xi, \eta)$ is a complex function, both the intensity as well as the phase can be calculated.

Also the real amplitude $O(x, y)$ of the object wave can be measured from the intensity by blocking the reference wave.

Example

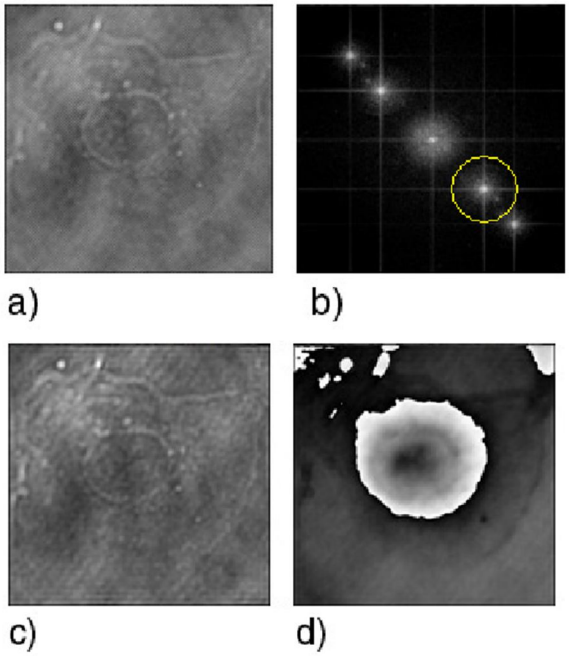

Figure 4

Figure 4 illustrates the implementation of the numerical algorithms in the reconstruction of an ovarian cell.

The area is $60 \times 60 \mu m^2$ with 424 x 424 pixels.

Figure 4(a) is the holographic interference pattern recorded by the CCD camera, and its Fourier transform in figure 4(b) is the angular spectrum.

A propagation phase factor $(z = 1.0 \mu m)$ is multiplied, and finally inverse-Fourier transformed to obtain the amplitude image in figure 4(c) and the phase image in figure 4(d).

The physical thickness of the cell can be calculated from

$$d = \lambda(\Delta\varphi / 2\pi) / (n - n_0) \quad \text{... (2.3)}$$

Where λ is the wavelength, $\Delta\varphi$ is the phase step and $(n - n_0)$ is the index difference between the film and air.

For example the layer of a cell is found to be about 110nm, assuming n=1.375.